Original Article | Genitourinary Imaging

https://doi.org/10.3348/kjr.2017.18.3.510
pISSN 1229-6929 · eISSN 2005-8330
Korean J Radiol 2017;18(3):510-518

Korean Journal of Radiology
KJR

Assessment of Cervical Cancer with a Parameter-Free Intravoxel Incoherent Motion Imaging Algorithm

Anton S. Becker, MD[1], Jose A. Perucho, BEng[2], Moritz C. Wurnig, MD, MSc[1], Andreas Boss, MD, PhD[1], Soleen Ghafoor, MD[1], Pek-Lan Khong, MD[2], Elaine Y. P. Lee, FRCR[2]

[1]Institute of Diagnostic and Interventional Radiology, University Hospital of Zurich, Zurich 8091, Switzerland; [2]Department of Diagnostic Radiology, The University of Hong Kong, Hong Kong, China

Objective: To evaluate the feasibility of a parameter-free intravoxel incoherent motion (IVIM) approach in cervical cancer, to assess the optimal b-value threshold, and to preliminarily examine differences in the derived perfusion and diffusion parameters for different histological cancer types.

Materials and Methods: After Institutional Review Board approval, 19 female patients (mean age, 54 years; age range, 37–78 years) gave consent and were enrolled in this prospective magnetic resonance imaging study. Clinical staging and biopsy results were obtained. Echo-planar diffusion weighted sequences at 13 b-values were acquired at 3 tesla field strength. Single-sliced region-of-interest IVIM analysis with adaptive b-value thresholds was applied to each tumor, yielding the optimal fit and the optimal parameters for pseudodiffusion (D*), perfusion fraction (F_p) and diffusion coefficient (D). Monoexponential apparent diffusion coefficient (ADC) was calculated for comparison with D.

Results: Biopsy revealed squamous cell carcinoma in 10 patients and adenocarcinoma in 9. The b-value threshold (median [interquartile range]) depended on the histological type and was 35 (22.5–50) s/mm^2 in squamous cell carcinoma and 150 (100–150) s/mm^2 in adenocarcinoma ($p < 0.05$). Comparing squamous cell vs. adenocarcinoma, D* (45.1 [25.1–60.4] x 10^{-3} mm^2/s vs. 12.4 [10.5–21.2] x 10^{-3} mm^2/s) and F_p (7.5% [7.0–9.0%] vs. 9.9% [9.0–11.4%]) differed significantly between the subtypes ($p < 0.02$), whereas D did not (0.89 [0.75–0.94] x 10^{-3} mm^2/s vs. 0.90 [0.82–0.97] x 10^{-3} mm^2/s, $p = 0.27$). The residuals did not differ (0.74 [0.60–0.92] vs. 0.94 [0.67–1.01], $p = 0.32$). The ADC systematically underestimated the magnitude of diffusion restriction compared to D ($p < 0.001$).

Conclusion: The parameter-free IVIM approach is feasible in cervical cancer. The b-value threshold and perfusion-related parameters depend on the tumor histology type.

Keywords: *Uterine cervical cancer; MRI; Diffusion MRI; Perfusion imaging; Technology assessment*

INTRODUCTION

Cervical cancer is the fourth most common cause of cancer related deaths in developed countries and the second most common cause in the third world countries (1). Recent advances in preventive medicine, namely human papillomavirus (HPV) vaccination and HPV-screening programs, have led to increased protection against cervical cancer (2). In diagnostics, there is a growing interest in the use of magnetic resonance imaging (MRI) for local staging

Received September 11, 2016; accepted after revision November 13, 2016.
This research was partially supported by the General Research Fund, Hong Kong (no. 17119916).
Corresponding author: Anton S. Becker, MD, Institute of Diagnostic and Interventional Radiology, University Hospital of Zurich, Raemistrasse 100, Zurich 8091, Switzerland.
• Tel: +41-44-255 1111 • Fax: +41-44-255 1819 • E-mail: anton.becker@usz.ch

Korean Journal of Radiology
KJR

(3). While patients with low-grade, locally confined tumors (Fédération de Gynécologie et d'Obstétrique [FIGO] stages IB1 and IIA1) may be amenable to surgical resection alone, advanced tumors require combined radio-chemotherapy (4). MRI not only provides detailed anatomical information but is also able to deliver functional information, e.g., about tissue diffusivity in diffusion weighted imaging (DWI). A promising approach is the intravoxel incoherent motion imaging (IVIM) analysis, which attempts to separate perfusion from true diffusion effects. In other words, the signal decay is described by a biexponential instead of a monoexponential equation which yields a more accurate description of the underlying tissue properties (5). IVIM has recently been shown to differentiate among histopathological tumor types, and, in addition, correlates with tumor grades of cervical cancer (6, 7).

Intravoxel incoherent motion imaging exploits a so-called "pseudodiffusion-effect" which corresponds to fast moving water molecules in the capillaries (5). This effect will, typically at low b-values (< 150 s/mm^2, though the exact threshold depends on the tissue), superimpose the signal decay caused by true diffusion. In the brain and kidney, IVIM derived perfusion parameters were reported to correlate with the blood flow measured *in-vivo* and *ex-vivo* (8). However, the conventional segmented biexponential fitting approach entails arbitrarily setting a b-value threshold for separating diffusion from perfusion decay (9). This requires *a priori* knowledge about the magnetization decay in the target tissue, and entails the danger of introducing a faulty physical property into the tissue analysis. In turn, an arbitrarily high or low b-value threshold will influence the derived diffusion and perfusion parameters (10) and create a potential confounder. A recently published parameter-free (i.e., with no *a priori* fixed parameters) IVIM fitting algorithm has shown promising results in the abdominal organs, yielding more stable perfusion and diffusion characterization of the liver, spleen, pancreas and kidney without the need of setting a b-value threshold (10). The algorithm has since been verified in neuroimaging as well (11). The algorithm essentially consists of computing an IVIM-fit for each b-value, one at a time. This will yield one possible curve or 'fit-candidate' for each acquired b-value (except the highest one, as explained below). By mathematically determining the best fit from those candidates, defined as the smallest sum of squared residuals to the curve/fit, one receives an optimal b-value threshold in addition to the "classical" IVIM parameters. Hence, under this paradigm, the b-value threshold is interpreted as an additional variable tissue specific marker.

The purpose of this study was to evaluate the feasibility of a parameter-free IVIM approach in cervical cancer, to assess the optimal b-value threshold, and to preliminarily examine differences in the derived perfusion and diffusion parameters for different histological cancer types.

MATERIALS AND METHODS

Patients

This prospective clinical study was approved by the local Institutional Review Board. After oral and written consent, 19 female patients (mean age, 54 years; range, 37–78 years) with biopsy-proven cervical cancer examined between June 2014 and December 2015 were enrolled. None of the patients had received prior treatment. Inability to cooperate, incomplete or non-diagnostic MRI scan were dropout criteria. Clinical FIGO stage was obtained from the patient's record.

Histopathological Analysis

Histopathological specimens were assessed by an experienced gynecological pathologist for tumor type and grade (G1–G3) and were subsequently reviewed at the weekly multi-disciplinary meeting.

Imaging Protocol

All patients were scanned on a clinical 3-tesla MRI scanner (Achieva 3T, Philips Healthcare, Best, the Netherlands), using a 16-channel phased array torso coil. Patients fasted for 6 hours prior to the examination and received 20 mg hyoscine butylbromide (Buscopan; Boehringer Ingelheim, Ingelheim am Rhein, Germany) as an intramuscular injection immediately before scanning to reduce bowel peristalsis. Diffusion datasets of the pelvis were acquired with a single-shot spin-echo echo-planar imaging sequence in axial orientation (20 slices) to include the entire cervical cancer using 13 b-values as suggested by Koh et al. (12): 0, 10, 20, 30, 40, 50, 75, 100, 150, 300, 500, 800, 1000 s/mm^2, in three orthogonal directions. Sequences were acquired in free breathing, and fat suppression was achieved by spectral presaturation with inversion recovery. Total scan time for the IVIM-sequence was approximately 6 minutes 30 seconds. Anatomical T1- and T2-weighted sequences, as summarized in Table 1, were acquired separately from the IVIM-sequence.

Table 1. Summary of MRI Scan Parameters

Sequences	T2W TSE	T2W TSE SPAIR	T2 TSE	T2W TSE	DWI	CE T1W-THRIVE
Plane	Sagittal	Coronal	Axial	Oblique axial	Axial	3D
TR/TE (ms)	4000/80	3500/80	2800/100	2800/100	2000/54	3/1.4
Turbo factor	30	21	12	14	NA	NA
FOV (mm)	240 x 240	230 x 230	402 x 300	220 x 220	406 x 300	370 x 203
Matrix size	480 x 298	352 x 300	787 x 600	316 x 311	168 x 124	248 x 134
Slice thickness (mm)	4	4	4	4	4	1.5
Intersection gap (mm)	0	0	0	0	0	0
Bandwidth (Hz/pixel)	230	186	169	162	15.3	724
NEX	2	1	1	1	2	1

CE = contrast-enhanced, DWI = diffusion-weighted imaging, FOV = field of view, NEX = number of excitation, SPAIR = spectral attenuated inversion recovery, THRIVE = T1W high resolution isotropic volume examination, TR/TE = repetition time/echo time, TSE = turbo spin echo

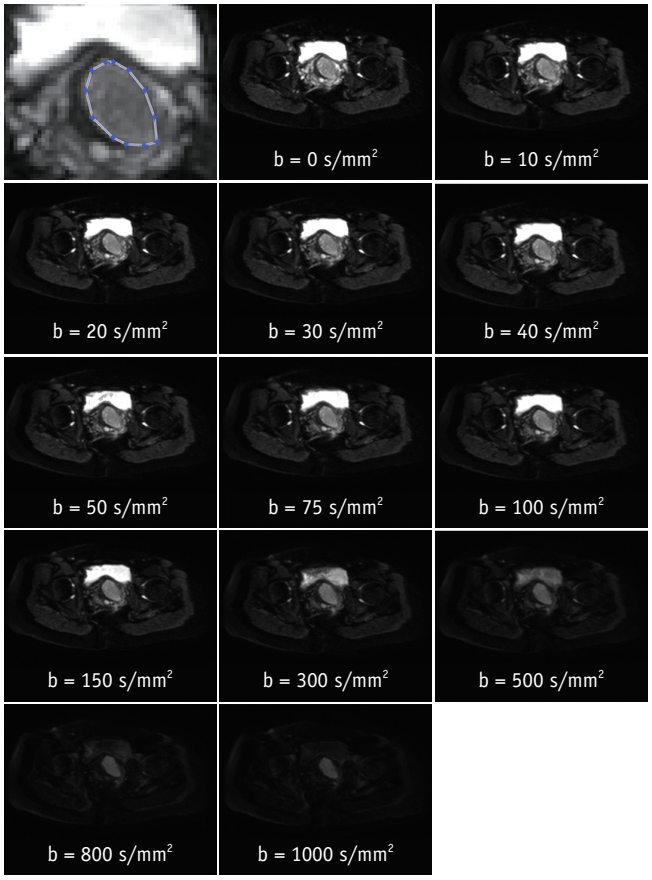

Fig. 1. ROI definition. Top left panel: screenshot of exemplary ROI definition in zoomed section of b_0 image (top row, middle). Remaining panels: diffusion signal decay series at single slice position of 53-year-old patient with adenocarcinoma arising from cervix. ROI = region of interest

Region-of-Interest Definition

For the analysis, polygonal regions-of-interest (ROI) in the tumor and in the gluteus maximus muscle were manually defined on the b = 0 s/mm² (b_0) image depicting the largest tumor diameter, and subsequently copied to the same position on the images of the remaining b-values of the same dataset. Necrotic areas, as well as prominent vessels, were avoided in order to assess only the actual tumor tissue. The absence of necrotic and vessel areas, as well as absence of obvious artifacts, was verified for all b-values. ROI definition was performed by a radiology resident and verified by a board-certified radiologist with 7 years of experience in genitourinary imaging. An exemplary ROI definition is shown in Figure 1. The obtained signal intensity curves were normalized to arbitrary units with the maximum value 1 at b_0.

For intra-reader agreement, the initial reader re-performed the ROI definition > 4 months after the initial analysis. For inter-reader agreement, a 2nd radiologist not involved in the original ROI definition, performed the same analysis independently.

IVIM Analysis

All IVIM-analyses were performed with optimized in-house MATLAB (Release 2015b, MathWorks, Natick, MA, USA) computer programs.

The IVIM approach tries to separate perfusion and diffusion effects in the signal decay by describing the decay with the following biexponential equation (Equation 1):

$$S_b/S_0 = (1-F_p)\exp(-bD) + F_p \exp(-bD^*)$$

S_b represents the signal at a given b-value, S_0 the signal at the b-value 0 s/mm², D the true molecular diffusion, D* the pseudodiffusion, and F_p the relative perfusion fraction.

The algorithm to compute the optimal b-value threshold and IVIM parameters is an extension of the adaptive b-value biexponential fitting, and has been published in detail before (10). In short, the following steps were performed:

I. Calculation of D from the highest n b-values with the assumption that perfusion contributions to the signal

Korean Journal of Radiology
KJR

decay are negligible at high b-values. First, n is equal to the number of all available b-values. D is calculated using a first-order polynomial fit to the log-transformed signal intensities (Equation 2):

$$\log S_b = -D \times b + \log S'_0$$

II. Calculation of F_p from the measured signal intensity at b = 0 (S_0) and the derived S_0' (Equation 3):

$$F_p = \frac{S_0 - S_0'}{S_0}$$

III. Calculation of D* (using the computed values for D and F_p as fixed factors) for all b-values by fitting the signal intensities to Equation 1 using a non-linear least-squares algorithm based on the Levenberg-Marquardt technique. The corresponding MATLAB function "lsqcurvefit" also provides the sum of the squared residuals to the fit.

IV. Steps I–III are repeated with the next lower b-value dropped in step I and II to determine the initial D and F_p. Thus, the algorithm will loop n-1 times (n = number of b-values). In the end, only the two highest b-values remain (for the highest b-value alone no polynomial fit can be calculated).

V. Finally, the optimal b-value threshold and corresponding IVIM-parameters are determined by determining the fit with the lowest number of squared residuals from step III, mathematically corresponding to the best fit to the measured signal intensities.

An illustration of several fits from the step-wise fitting process is depicted in Figure 2.

Furthermore, a conventional monoexponential apparent diffusion coefficient (ADC) was computed from two b-values (0 and 800 s/mm^2) for comparison with D.

In addition to the ROI analysis, voxel-wise IVIM analysis of the selected slices was done to generate parametrical b-value threshold, F_p-, D-, and D*-maps of the whole examined region as a visual instrument to verify the quantitative measurements obtained by the ROI analysis.

Statistical Analysis

Statistical analysis was performed using R version 3.2.4. (R Foundation for Statistical Computing, Vienna, Austria). Medians and interquartile ranges (IQR) of the IVIM parameters F_p, D, and D* as well as the optimal b-value threshold, defined as the b-value threshold resulting in the fit with the smallest sum of squared residuals, were computed for muscle, squamous cell carcinomas and for adenocarcinomas. Intra- and inter-reader agreements were assessed with a weighted Cohen's kappa (κ). The κ scores were interpreted as follows: slight ($\kappa < 0.20$), fair ($\kappa = 0.20–0.39$), moderate ($\kappa = 0.40–0.59$), substantial ($\kappa = 0.60–0.79$), or excellent ($\kappa > 0.80$) agreement (13). Correlations were assessed with a Pearson correlation coefficient for the clinical FIGO stage and histological differentiation. Since normality for the calculated parameters could not be assumed, the results were

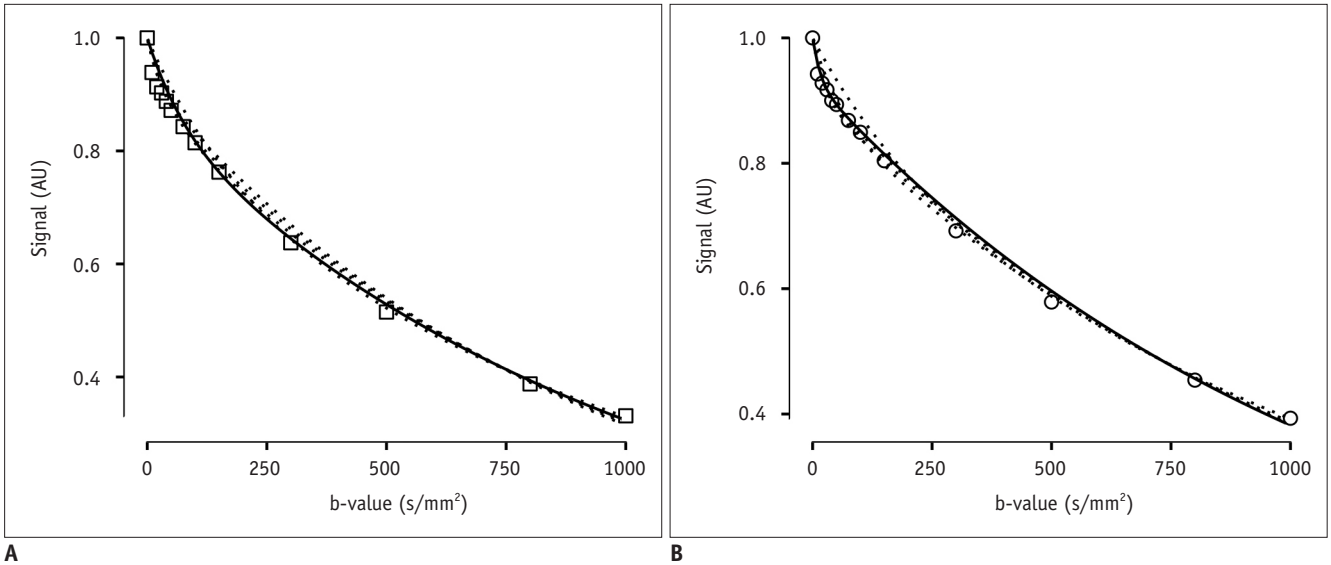

Fig. 2. Example signal decay with fitted curve candidates at different b-value thresholds (dotted lines).
Best fit, i.e., curve with smallest sum of squared residuals, is drawn as continuous line (b-value threshold = 150 s/mm^2 in **(A)**, and 10 s/mm^2 in **(B)**). One sample of adenocarcinoma is shown in **(A)**, sample of squamous cell carcinoma is shown in **(B)**. Signal is given in arbitrary units (AU) normalized to maximum of 1 and minimum of 0.

compared with a Wilcoxon rank sum test. A significance level of $p < 0.05$ was considered statistically significant, and p values were corrected for multiple comparisons with the Benjamini-Hochberg procedure (14). Significantly different parameters were further assessed with a receiver operator characteristics (ROC) analysis. All plots including an exemplary fitting process were plotted with ggplot2 (15) from the MATLAB output.

RESULTS

There were 7 patients with a FIGO-stage I, 8 patients with a stage II, and 4 patients with a stage III tumor. Ten patients had squamous cell carcinomas, and 9 patients had adenocarcinomas. Only 2 patients had low-grade tumors (G1, well differentiated); 7 patients, intermediate (G2, moderately differentiated); 2 patients, intermediate to high (G2–3); and 4 patients, high-grade (G3, poorly differentiated) tumors. Accurate grading was not possible in 4 tumors (GX).

Image acquisition and post-processing were successfully completed for all patients.

Intra-reader agreement was substantial for D {$\kappa = 0.79$ (95% confidence interval [CI]: 0.57–1.0)} and moderate for F_p (0.50 [0.15–0.84]) and D* (0.57 [0.21–0.93]). Similarly, inter-reader agreement was substantial for D ($\kappa = 0.67$ [95% CI: 0.37–0.98] and moderate for F_p (0.53 [0.18–0.87]) and D* (0.52 [0.26–0.78]).

The highest b-value threshold was found in the paraspinal muscle (median 500 s/mm^2 [IQR: 40–500 s/mm^2]), with a D = 1.40 (1.34–1.43) x 10^{-3} mm^2/s, D* = 5.7 (5.2–25.7) x 10^{-3} mm^2/s and F_p = 10.5% (8.1–12.3%). Squamous cell carcinomas, compared to adenocarcinomas, exhibited a significantly higher D* (45.1 [25.1–60.4] vs. 12.4 [10.5–21.2] x 10^{-3} mm^2/s, adjusted $p = 0.03$), lower F_p (7.5% [7.0–9.0%] vs. 9.9% [9.0–11.4%]) and lower b-value threshold (35 [22.5–50] s/mm^2 vs. 150 [100–150] s/mm^2, $p = 0.03$) (Table 2, Figs. 3, 4). The sum of squared residuals was not significantly different between the adenocarcinoma and the squamous cell carcinoma group ($p = 0.3$).

Table 2. IVIM Parameters and Sum of Squared Residuals for Two Carcinoma Types and Muscle Tissue

	D* (x 10^{-3} mm^2/s)	F_p (%)	D (x 10^{-3} mm^2/s)	b-Value Threshold (s/mm^2)	Residuals
Muscle	5.7 (5.2–25.7)	10.5 (8.1–12.3)	1.40 (1.34–1.43)	500 (40–500)	0.29 (0.18–0.62)
Squamous cell carcinoma	45.1 (25.1–60.4)	7.5 (7.0–9.0)	0.89 (0.75–0.94)	35 (22.5–50)	0.74 (0.60–0.92)
Adenocarcinoma	12.4 (10.5–21.2)	9.9 (9.0–11.4)	0.90 (0.82–0.97)	150 (100–150)	0.94 (0.67–1.01)

Data are median (interquartile range). IVIM = intravoxel incoherent motion

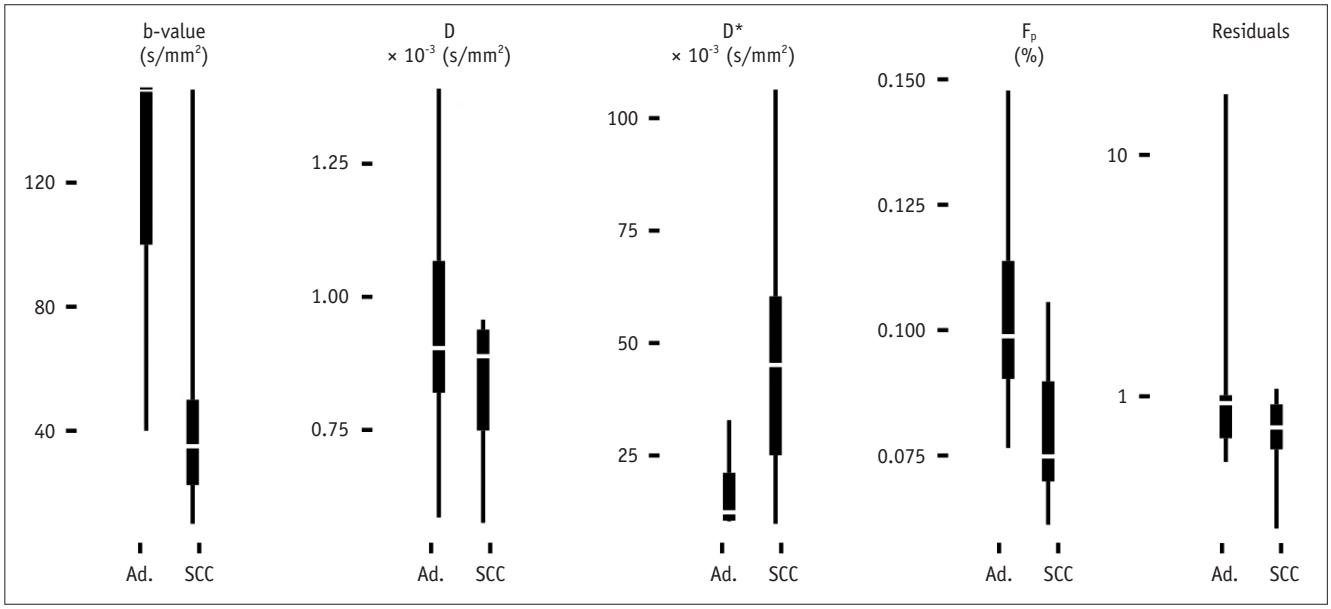

Fig. 3. Boxplot of optimal b-value thresholds (defined as yielding smallest sum of squared residuals to fit, which are depicted on far right as "residuals") and IVIM parameters D, D*, and F_p of two examined histological cancer types adenocarcinoma (Ad.) and squamous cell carcinoma (SCC). IVIM = intravoxel incoherent motion

Korean Journal of Radiology
KJR

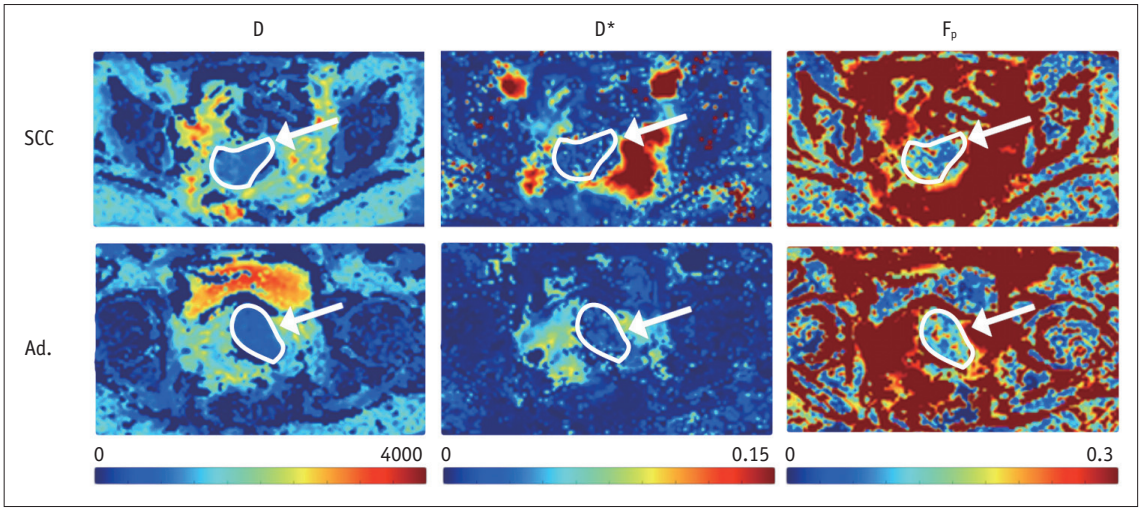

Fig. 4. Parametric maps depicting three IVIM parameters D, D*, and F_p in one case of squamous cell carcinoma (SCC) in top row, and adenocarcinoma (Ad.) in bottom row (both outlined and marked with white arrow). Difference in F_p is subtle, but can be appreciated in right column with color scale set to maximum of 0.3 for this example. IVIM = intravoxel incoherent motion

Table 3. Results of Pearson Correlation Test for FIGO-Stages and Histological Grades

	FIGO Stage	Histologic Grades
r (D*)	0.51	0.30
p (D*)	0.03	0.28
ad-*p* (D*)	0.08	0.51
r (F_p)	-0.48	-0.24
p (F_p)	0.04	0.38
ad-*p* (F_p)	0.08	0.51
r (D)	-0.01	-0.14
p (D)	0.97	0.61
ad-*p* (D)	0.97	0.61
r (b-value threshold)	-0.39	-0.47
p (b-value threshold)	0.10	0.08
ad-*p* (b-value threshold)	0.12	0.32

r = correlation coefficient; i.e., slope of correlation line; *p* = raw *p* value; ad-*p* = adjusted *p*; i.e., adjusted for multiple comparisons. FIGO = Fédération de Gynécologie et d'Obstétrique

Although Pearson correlation testing initially showed promising results, namely D* and F_p correlating with the FIGO stage (correlation coefficient $r = 0.51$ and -0.48, respectively), the results have to be considered non-significant after correcting for multiple comparisons (adjusted $p = 0.08$). Both the b-value threshold and D did not correlate significantly with either FIGO stage or histological grade ($p > 0.05$) (Table 3).

Receiver operator characteristics curve analysis demonstrated areas under the curve (A_z) for F_p and D* of 0.82 and 0.81, respectively, and 0.78 for the b-value threshold. The cutoff for F_p was 0.1 (sensitivity 50% [20–80%; bootstrapped 95%-CI], specificity 100%), for D* 37.8 x 10^{-3} mm^2/s (sensitivity, 60% [30–90%]; specificity, 100%) and for the b-value 75 s/mm^2 (sensitivity, 80% [50–100%]; specificity, 77.8% [44–100%]). An illustration of the three ROC-curves is depicted in Figure 5.

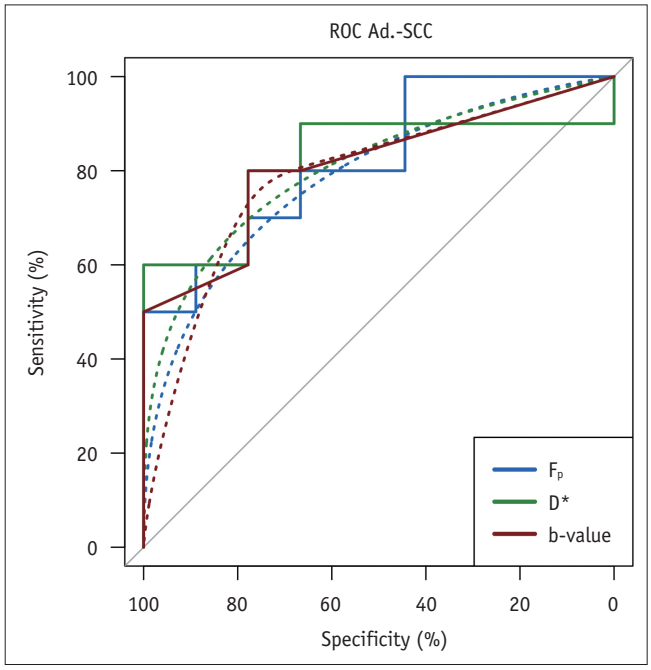

Fig. 5. Receiver operator characteristics curve of three IVIM derived parameters for differentiation of adenocarcinoma (Ad.) and squamous cell carcinoma (SCC). A_z was 0.82 (F_p, D*) and 0.81 (b-value threshold). IVIM = intravoxel incoherent motion

The ADC derived from the monoexponential model (1.01 [0.95–1.20] x 10^{-3} mm^2/s) systematically underestimated the diffusion restriction compared to D (0.90 [0.84–0.95] x 10^{-3} mm^2/s, $p < 0.001$) due to contamination with perfusion

related signal decay at low b-values (Supplementary Fig. 1 in the online-only Data Supplement). Although the difference between ADC and D tended to be larger in adenocarcinomas (0.17) compared to squamous cell carcinomas (0.11), this discrepancy was not significant (p = 0.13).

DISCUSSION

This study found that the parameter-free IVIM approach is feasible in MRI of cervical cancer, and that the optimal b-value threshold lies between 20 and 150 s/mm^2, but seems to be dependent on the histological type of the tumor. Squamous cell cancers cluster around 30 ± 20 s/mm^2, and adenocarcinomas lean heavily towards the higher end of the spectrum at 150 s/mm^2. In addition, D* and F_p differed significantly between the two histology types. The sum of squared residuals, however, did not differ significantly between the two types, suggesting that the derived IVIM parameters accurately described the measured signal decay. Moreover, the b-value thresholds in the paraspinal muscle are in line with previous reports (10), showing the relative stability of the algorithm across platforms. In the conventional segmented biexponential fitting approach with an *a priori* selected, fixed b-value threshold, D* tended to be "unstable" due to an arbitrarily chosen b-value that did not correspond to the true physical properties of the tissue, because the derived IVIM parameters depend heavily on the b-value threshold used (10). Previously, D* did not even allow for differentiation between normal and cancerous tissue because of its high variability (7). The present finding that the ADC tends to underestimate perfusion restriction is consistent with results of a more extensive study demonstrating that parameters derived from a monoexponential model are clearly inferior in the differentiation of cervical cancer when compared to parameters from biexponential models such as IVIM (16). This implies that a reliable IVIM algorithm is of particular interest for cervical carcinoma.

F_p has been found to correlate with dynamic contrast-enhanced MRI in cervical cancer (17). Adenocarcinomas of the cervix exhibit a higher expression of vascular endothelial growth factor and thus a higher density of microvasculature in the tumor stroma (18) when compared to squamous cell cancer or the normal cervix uteri (19). This is in agreement with the higher F_p found in the adenocarcinomas in this study. On the other hand, the pseudodiffusion coefficient, D*, has been shown to correlate directly with the histologic microvessel count in the abdominal organs of healthy mice (20), as well as in a colon cancer xenograft model (21). Due to its instability in the conventional biexponential fitting approach, however, it is rarely investigated as a surrogate marker in clinical research. Somewhat surprisingly a lower D* was found in the adenocarcinomas in this study. Unfortunately, the histological specimens were not analyzed for microvessel density with a special staining. However, this lack will be addressed in a future study. It is likely that the low D* may be a reflection of abnormal blood flow due to the pathologic, irregular tumor vessels, which may behave differently from the physiological vasculature or vessels of other tumor entities.

In summary, the parameter-free IVIM algorithm seems to yield a stable D* and F_p as potential surrogate markers of tumor microcirculation or architecture. It may thus be able to preoperatively assess the histologic type based on differences in IVIM parameters. The ability to discriminate between tumor types is of great clinical interest, since the Pap smear will often miss adenocarcinomas, which preferentially exhibit an endocervical growth pattern. The baseline treatment generally depends on staging and not tumor histology. However, the histopathological subtype is an independent predictor for outcome, patterns of failure after primary treatment, and response to specific treatments, in addition to other well-known prognostic factors like parametrial invasion, resection margins and nodal status (22). This in turn, has an impact on adjuvant treatment planning and oncological follow-up strategies (23, 24). When combined with other techniques such as ^{1}H MR spectroscopy, which has recently been shown to accurately predict the HPV genotype in cervical cancer (25), IVIM may be useful in the future for assessing the "MR fingerprint" of a cancer and predicting more accurately the histological and molecular tumor characteristics from the radiological data.

This study has two major limitations that need to be acknowledged. First, the IVIM analysis was performed on a single slice with the largest tumor diameter, and not on multiple slices evaluating the whole tumor volume. Since this method does not incorporate tumor heterogeneity but uses the averaged ROI content, it would probably not benefit from whole-tumor-analysis. However, our parameter-free algorithm will be implemented for whole-tumor analysis in further studies. Second, only a small number of patients were analyzed. Nevertheless, the group size of this methodological pilot study was large enough to detect

Korean Journal of Radiology
KJR

significant differences in the b-value threshold between different types of cervical cancer. For the comparison between the histological types, the power of these findings is certainly low and an extended study including more patients to investigate IVIM parameters as possible surrogate markers will be undertaken. The small cohort size is a possible explanation for the lack of significant correlations with the FIGO-stage and tumor differentiation, both of which have been established before (6, 26).

One of the major obstacles preventing the widespread clinical use of IVIM is the long duration of the scan protocol due to the need to acquire images at numerous b-values (27, 28). Based on the present data, it may be feasible to add two or three b-values (e.g., 30, 80, and 150 s/mm^2) to a clinical pelvic DWI protocol, thus making it accessible for IVIM analysis. The accuracy of such a protocol would have to be evaluated in further studies.

In conclusion, the parameter-free IVIM approach is feasible in cervical cancer. The optimal b-value threshold, as well as the derived parameters D* and F_p, appear to depend on the histological type of tumor.

Supplementary Materials

The online-only Data Supplement is available with this article at https://doi.org/10.3348/kjr.2017.18.3.510.

REFERENCES

1. Torre LA, Bray F, Siegel RL, Ferlay J, Lortet-Tieulent J, Jemal A. Global cancer statistics, 2012. *CA Cancer J Clin* 2015;65:87-108
2. Ronco G, Dillner J, Elfström KM, Tunesi S, Snijders PJ, Arbyn M, et al. Efficacy of HPV-based screening for prevention of invasive cervical cancer: follow-up of four European randomised controlled trials. *Lancet* 2014;383:524-532
3. Wakefield JC, Downey K, Kyriazi S, deSouza NM. New MR techniques in gynecologic cancer. *AJR Am J Roentgenol* 2013;200:249-260
4. Koh WJ, Greer BE, Abu-Rustum NR, Apte SM, Campos SM, Chan J, et al. Cervical cancer. *J Natl Compr Canc Netw* 2013;11:320-343
5. Le Bihan D, Breton E, Lallemand D, Aubin ML, Vignaud J, Laval-Jeantet M. Separation of diffusion and perfusion in intravoxel incoherent motion MR imaging. *Radiology* 1988;168:497-505
6. Zhou Y, Liu J, Liu C, Jia J, Li N, Xie L, et al. Intravoxel incoherent motion diffusion weighted MRI of cervical cancer -correlated with tumor differentiation and perfusion. *Magn Reson Imaging* 2016;34:1050-1056
7. Lee EY, Yu X, Chu MM, Ngan HY, Siu SW, Soong IS, et al. Perfusion and diffusion characteristics of cervical cancer based on intraxovel incoherent motion MR imaging-a pilot study. *Eur Radiol* 2014;24:1506-1513
8. Lorenz CH, Pickens DR 3rd, Puffer DB, Price RR. Magnetic resonance diffusion/perfusion phantom experiments. *Magn Reson Med* 1991;19:254-260
9. Alison M, Chalouhi GE, Autret G, Balvay D, Thiam R, Salomon LJ, et al. Use of intravoxel incoherent motion MR imaging to assess placental perfusion in a murine model of placental insufficiency. *Invest Radiol* 2013;48:17-23
10. Wurnig MC, Donati OF, Ulbrich E, Filli L, Kenkel D, Thoeny HC, et al. Systematic analysis of the intravoxel incoherent motion threshold separating perfusion and diffusion effects: proposal of a standardized algorithm. *Magn Reson Med* 2015;74:1414-1422
11. Stieb S, Boss A, Wurnig MC, Özbay PS, Weiss T, Guckenberger M, et al. Non-parametric intravoxel incoherent motion analysis in patients with intracranial lesions: test-retest reliability and correlation with arterial spin labeling. *Neuroimage Clin* 2016;11:780-788
12. Koh DM, Collins DJ, Orton MR. Intravoxel incoherent motion in body diffusion-weighted MRI: reality and challenges. *AJR Am J Roentgenol* 2011;196:1351-1361
13. Landis JR, King TS, Choi JW, Chinchilli VM, Koch GG. Measures of agreement and concordance with clinical research applications. *Stat Biopharm Res* 2012;3:185-209
14. Benjamini Y, Hochberg Y. Controlling the false discovery rate: a practical and powerful approach to multiple testing. *J R Stat Soc Ser B (Methodol)* 1995;57:289-300
15. Wickham H. *Ggplot2: elegant graphics for data analysis*. New York: Springer Science & Business Media, 2009
16. Winfield JM, Orton MR, Collins DJ, Ind TE, Attygalle A, Hazell S, et al. Separation of type and grade in cervical tumours using non-mono-exponential models of diffusion-weighted MRI. *Eur Radiol* 2017;27:627-636
17. Lee EY, Hui ES, Chan KK, Tse KY, Kwong WK, Chang TY, et al. Relationship between intravoxel incoherent motion diffusion-weighted MRI and dynamic contrast-enhanced MRI in tissue perfusion of cervical cancers. *J Magn Reson Imaging* 2015;42:454-459
18. Fujimoto J, Sakaguchi H, Hirose R, Ichigo S, Tamaya T. Expression of vascular endothelial growth factor (VEGF) and its mRNA in uterine cervical cancers. *Br J Cancer* 1999;80:827-833
19. Saijo Y, Furumoto H, Yoshida K, Nishimura M, Irahara M. Clinical significance of vascular endothelial growth factor expression and microvessel density in invasive cervical cancer. *J Med Invest* 2015;62:154-160
20. Eberhardt C, Wurnig MC, Wirsching A, Rossi C, Rottmar M, Özbay PS, et al. Intravoxel incoherent motion analysis of abdominal organs: computation of reference parameters in a large cohort of C57Bl/6 mice and correlation to microvessel density. *MAGMA* 2016;29:751-763
21. Lee HJ, Rha SY, Chung YE, Shim HS, Kim YJ, Hur J, et al. Tumor perfusion-related parameter of diffusion-weighted magnetic resonance imaging: correlation with histological microvessel density. *Magn Reson Med* 2014;71:1554-1558
22. Shimada M, Nishimura R, Nogawa T, Hatae M, Takehara K,

Yamada H, et al. Comparison of the outcome between cervical adenocarcinoma and squamous cell carcinoma patients with adjuvant radiotherapy following radical surgery: SGSG/TGCU Intergroup Surveillance. *Mol Clin Oncol* 2013;1:780-784
23. Katanyoo K, Sanguanrungsirikul S, Manusirivithaya S. Comparison of treatment outcomes between squamous cell carcinoma and adenocarcinoma in locally advanced cervical cancer. *Gynecol Oncol* 2012;125:292-296
24. Galic V, Herzog TJ, Lewin SN, Neugut AI, Burke WM, Lu YS, et al. Prognostic significance of adenocarcinoma histology in women with cervical cancer. *Gynecol Oncol* 2012;125:287-291
25. Lin G, Lai CH, Tsai SY, Lin YC, Huang YT, Wu RC, et al. 1H MR spectroscopy in cervical carcinoma using external phase array body coil at 3.0 Tesla: prediction of poor prognostic human papillomavirus genotypes. *J Magn Reson Imaging* 2017;45:899-907
26. McVeigh PZ, Syed AM, Milosevic M, Fyles A, Haider MA. Diffusion-weighted MRI in cervical cancer. *Eur Radiol* 2008;18:1058-1064
27. Lemke A, Stieltjes B, Schad LR, Laun FB. Toward an optimal distribution of b values for intravoxel incoherent motion imaging. *Magn Reson Imaging* 2011;29:766-776
28. Lemke A, Laun FB, Klauss M, Re TJ, Simon D, Delorme S, et al. Differentiation of pancreas carcinoma from healthy pancreatic tissue using multiple b-values: comparison of apparent diffusion coefficient and intravoxel incoherent motion derived parameters. *Invest Radiol* 2009;44:769-775